# Spectrally Focused Markov Random Field Image Modeling in 3D CT

Jiao Wang, Ken Sauer, *Member, IEEE*, Jean-Baptiste Thibault, *Member, IEEE*, Zhou Yu, *Member, IEEE*, and Charles Bouman, *Fellow, IEEE*

***Abstract*—Markov random fields (MRFs) are a broadly useful and relatively economical stochastic model for imagery in Bayesian estimation. The simplicity of their most common examples allows local computation in iterative optimization, and statistical descriptions of image ensembles which discourage dramatic behavior, particularly under models with strictly convex potential functions. This simplicity may be a liability, however, when the inherent bias of minimum mean-squared error or maximum *a posteriori* probability (MAP) estimators attenuate all but the lowest spatial frequencies. For applications where more flexibility in spectral response is desired, potential benefit exists in models which accord higher *a priori* probabilities to content in higher frequencies. This paper illustrates the gains possible with MRF design similar to inner bone emphasis in conventional X-ray CT reconstruction.**

## I. Introduction

X-ray CT imaging appears to be a rich potential field of application for iterative reconstruction techniques [1]–[6]. Among the approaches promoted for clinical application, several take advantage of *a priori* image modeling in the Bayesian estimation view of the problem, in which the regularization function has an probabilistic interpretation. The Markov random field (MRF) model has long played a prominent role in this sort of Bayesian image estimation. It is economical in its parameterization of multidimensional random phenomena, but provides a powerful ensemble of models and effective regularization in inverse problems. A generic Gibbs distribution, whose equivalence to the MRF is established by the Hammersly-Clifford Theorem [7], has the form

$$p_X(x) = Z^{-1} \exp(-U(x)). \tag{1}$$

The normalization constant $Z$ is essential in MRF parameter estimation, but is not of great interest in the present setting, where we estimate only the image. In most common MRFs, the probability measure for the realization $x$ of the random field $X$ may be written in the form

$$U(x) = \gamma \sum_{\{i,j\}\in\Omega} w_{i,j}\rho(x_i - x_j), \tag{2}$$

Jiao Wang and Ken Sauer are with the Department of Electrical Engineering, University of Notre Dame, Notre Dame, IN 46556, USA; E-mail: sauer@nd.edu, phone: 574-631-6999.
Jean-Baptiste Thibault and Zhou Yu are with the Applied Science Laboratory, GE Healthcare, Waukesha, WI 53188, USA; E-mail: jean-baptiste.thibault@med.ge.com, zhou.yu@med.ge.com.
Charles Bouman is with the Department of Electrical and Computer Engineering, Purdue University, West Lafayette, IN 47907, USA; E-mail: bouman@purdue.edu.

with $\Omega$ the collection of cliques describing the neighborhood of each pixel, $\{w_{i,j}\}$ the set of weights for penalizing local differences according to relative spatial locations, $\gamma$ a scaling factor, and $\rho(\cdot)$ describing the penalty as a function of the magnitude of local pixel differences.

The set $\{w_{i,j}\}$ is typically chosen to penalize differences between pairs of image pixels inversely proportionally to distance between sites, or some such minimally committal form. Gauss-Markov models [8] feature a log prior of

$$\log p_X(x) = -(1/2)\gamma x^T R x + constant, \tag{3}$$

which incorporates inverse spatial covariance of the model into the matrix $R$, equivalently considered the regularizing norm. The implicit spectral model of $X$ is therefore the inverse of the power spectral density modeled by $R$. Second-order MRFs meant to be invariant to rotation have essentially one degree of freedom in choosing the weighting coefficients: the ratio of diagonal to horizontal and vertical weights. This limits spectral description to a crude low-pass model.

In this paper we explore the potential of larger neighborhoods in MRFs considered from the point of view of probabilistic modeling of spatial frequency content. This leads naturally to the inclusion of frequency response in the design of stochastic inverse operators, and is useful for the design of explicit characteristic image behavior such as noise and spatial resolution trade-off for practical applications. We consider particularly the preservation of detail in bone structure in X-ray CT.

## II. Frequency Response in Linearized Inverse

While we may apply new stochastic models with both quadratic and non-quadratic penalties in the function $\rho$ of (2), we begin with linear analysis for approximation of the frequency response characteristics of inverse operators. Consider the inverse problem posed by

$$y = Ax + n, \tag{4}$$

in which the distribution of the noise in $n$ dictates a quadratic log-likelihood function with norming matrix (e.g. inverse covariance) $D$. Under quadratic MRFs as described above, the maximum *a posteriori* probability estimate, which coincides with the minimum mean-squared error (MMSE) estimate of $x$, is

$$\hat{x} = (A^T D A + \gamma R)^{-1} A^T D y. \tag{5}$$

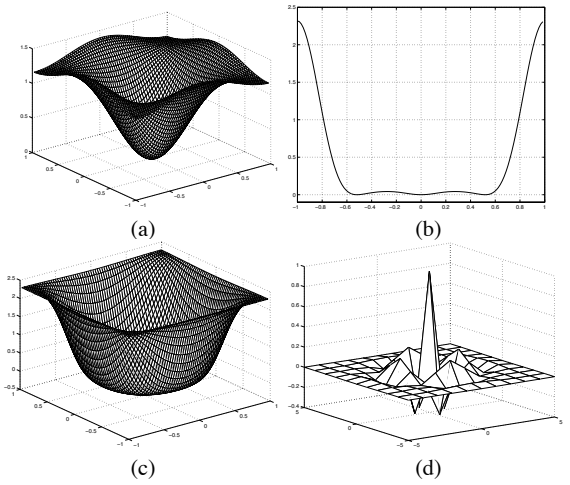

Fig. 1. (a) Two-dimensional $R(\omega)$ for conventional 2nd-order MRF; (b) 1-D FIR design for frequency emphasis near 0.5. (c) $R(\omega)$ from McClellan transformation of 1-D filter; (d) corresponding MRF clique weights.

In this case, using a frequency-domain representation of the total transformation, the system response to $x$ is

$$G(\omega) = \frac{A_D(\omega)}{A_D(\omega) + \gamma R(\omega)}, \tag{6}$$

where $A_D(\omega)$ is a local spectral representation of the operator $A^T D A$, and the filter exhibits the familiar Fourier representation of the Wiener filter for shift-invariant linear filtering as solution to the estimation problem. The bias toward zero of the estimate of each frequency component in $\hat{x}$ is observed as

$$\frac{\gamma R(\omega)}{A_D(\omega) + \gamma R(\omega)}.$$

That is the reduction of magnitude according to noise-to-signal ratio in the pursuit of MMSE at each frequency.

Particularly if we wish to make the estimator adaptive to local texture or boundaries, large *a priori* probabilities of prominent narrow-band signal components may be appropriate. Conditioned on detection of a known texture category through either hard or soft classification, or in objects characterized by presence of strong elements of a known frequency band, it may be desirable to suppress noise differentially by an $R(\omega)$ which treats specific frequencies as having high probability. The very simple spectral model of the signal to be recovered which is implied by low-order MRF models allows little tuning of the inverse operator to specific spectral characteristics. Expanding the number of two-member cliques enriches the *a priori* modeling greatly in its ability to focus spectral characteristics.

Figure 1 includes a simple example in two dimensions. The most common formulation of 2nd-order MRF weights implies the inverse signal power spectral density on the top left. The estimator resulting from this image model strongly attenuates the normalized frequencies above 0.3. As is obvious in (5), the linear least-squared error estimator biases the signal only toward zero, as all components of the expression are positive. Within conventional estimation, this is desirable, but if perceived image qualities become more important than quantitative measure, or if a particular spectral component's amplification is desired for greater visibility, negative values in $R(\omega)$ present another option. This notion immediately challenges the stochastic image model's correctness, as it contradicts the non-negative definiteness of the autocorrelation, and makes the *a priori* image model decidedly improper. However, we observe that the great majority of MRFs, which penalize only pixel differences, are also improper probability densities. In the Gaussian case, this penalty presents a rank-deficient inverse covariance matrix. Improper densities are routinely and profitably applied in Bayesian estimation [9], with reliance on combination with likelihood functions to formulate stable estimates. From the equations above, we note that the condition

$$\gamma R(\omega) > -A_D(\omega) \tag{7}$$

maintains stability in the MAP estimate provided the *a posteriori* density is viable for the entire observation space of $Y$.

As an example, consider the inverse (improper) spectral density $R(\omega)$ shown in Figure 1. This function is constructed through one-dimensional non-uniformly spaced frequency sampling design, with negative values between normalized frequency 0.5 and 0.6, intended to boost intermediate frequency components. The resulting filter in Fig. 1(b) is transformed into an $11 \times 11$ two-dimensional equivalent via the McClellan transform to form the function $R(\omega)$ of Fig. 1(c). The corresponding set of coefficients in Fig. 1(d) includes negative values, which positively sanction some larger local differences.

## III. Non-Quadratic Models

Non-Gaussian MRFs do not strictly follow the linear analysis of estimator forms and properties explained above. Nonetheless, we will attempt to exploit what we learn in the linear case to extend these ideas to Bayesian estimation under more general models. Despite differences in the energy function and consequent variation in rendering of discontinuities, we conjecture that the spatial frequency properties of the linear case will to a great degree be shared by nonlinear estimates.

Much innovation has been focused on the function $\rho(\cdot)$, with the classical quadratic smoothing penalty often replaced by alternatives which penalize large differences less dramatically in order to better preserve discontinuities in pixel values [10], [11]. Strict convexity of the negative log *a posteriori* probability density is highly desirable for reliable convergence and stable estimation. At a minimum, positive-definiteness of the Hessian of the negative log *a priori* density requires the diagonal terms satisfy

$$\sum_{i \in \mathcal{N}_j} w_{ij} \frac{\partial^2}{\partial x_j^2} \rho(x_j - x_i) \geq 0 \tag{8}$$

over the entire feasible set for the image $X$. $\mathcal{N}_j$ is the neighborhood of pixel $j$, composed of all pixels which are part of cliques including site $j$.

For image quality and favorable numerical behavior, forcing $\rho(\cdot)$ to have quadratic shape at the origin has proven valuable. We have found the q-Generalized Gaussian MRF (q-GGMRF) [12], with

$$\rho(\Delta) = \frac{|\Delta|^p}{1 + |\Delta/c|^{p-q}}, \tag{9}$$

to provide both appropriate low-intensity smoothing as well as edge preservation. The parameter $q$ forms the penalty for large differences, and is typically chosen near 1.2, with $p = 2$. The threshold $c$ determines the location of approximate transition from low-intensity, Gaussian behavior to edge mode. This model features an upper bound on the individual second derivatives in (8) and therefore relatively simple conditions for meeting (8) on a reasonable feasible set. These conditions are quite restrictive for the q-GGMRF, and for such designs as featured in Fig. 1(d), we sacrifice the convexity of the log prior. Though the total log *a posteriori* probability may remain convex in most regions of interest, we expect it will be non-convex in sparsely sampled regions, where the likelihood term is relatively weak.

In order to accelerate each voxel update in ICD algorithm, we have proposed a 1D optimization using a quadratic substitute function to upper bound the local 1D log prior function [6]. We form the substitute function by replacing each function $\rho(x_i - x_j)$ in (2) with $f_{ij}(u)$. The function $f_{ij}(u)$ is chosen to have a simple quadratic form

$$f_{ij}(u) = a_{ij}u^2 + b_{ij}u + c_{ij}, \tag{10}$$

so that it is easy to minimize. Let $\tilde{x_j}$ be the current state of the voxel whose value is to be optimized. The coefficients $a_{ij}$, $b_{ij}$, $c_{ij}$ are chosen such that $f_{ij}(u)$ and $\rho(x_i - u)$ are tangent to each other at $u = \tilde{x_j}$ and $f_{ij}(u)$ is greater than or equal to $\rho(x_i - u)$ for all $u$. With non-negative $w_{ij}$, this substitution guarantees descent of the true cost function with simplified computation of the derivatives of $f$. In the presence of negative weights resulting from our MRF spectral design, we propose a modified substitute function with a simple linear form

$$f_{ij}(u) = \begin{cases} a_{ij}u^2 + b_{ij}u + c_{ij}, & w_{ij} \geq 0 \\ b_{ij}u + c_{ij}, & w_{ij} < 0, \end{cases} \tag{11}$$

so that the convexity of the substitute log prior is guaranteed by giving the sub-function properties above to the components of $U(x)$ having negative coefficients. Although the true cost function may be non-convex, this modified substitute function guarantees monotonic descent to at least a local minimum of the true cost.

## IV. MRF Design Applied to X-ray CT

We apply the MRF design above to Bayesian three-dimensional reconstruction from axial X-ray CT scans on a GE LightSpeed VCT scanner. While the reconstructions are fully three-dimensional, our expanded MRF design is restricted to the transaxial direction; in the axial direction we use a conventional, first-order Markov description in a separable model. Similar design, however, may easily be applied in three dimensions.

The data producing Figure 2(a) are combined from multiple realizations of acquisitions taken at the highest available dose setting to form a scan set equivalent to a single very high dose acquisition, providing accurate detail in a conventional filtered backprojection (FBP) reconstruction. We therefore view the first image as "ground truth" in this experiment. FBP allows linear filter selection for varying frequency response shapes, with Fig. 2(b) image illustrating a choice emphasizing interior bone structure. In the first Bayesian reconstruction, we apply the q-GGMRF with a conventional $3 \times 3$ neighborhood in the $(x, y)$ plane. This model has proven effective in broad clinical applications but, for the particular choice of parameters shown in Fig. 2(c), limits detail content in the trabecular bone regions.

For a first case with the spectral MRF design, we consider the linear case resulting from the quadratic *a priori*. We use the coefficients from Figure 1 for the in-plane regularization. Although $R(\omega)$ is negative at some frequencies, the response in (6) is everywhere positive, and the estimate is well-posed. The result in Fig. 2(d) shows an emphasis of the typical inner bone frequencies similar to that of bone-enhanced FBP, while still suppressing noise at the higher frequencies. Thus in this case, we see the potential to fruitfully control frequency response of the Bayesian inverse operator.

An axial clinical scan appears in Figure 3. The first image again illustrates the result of conventional MAP reconstruction under the q-GGMRF, small-neighborhood prior, with good noise suppression, soft tissue rendering, and high frequency bone detail such as in the inner ear, but limited trabecular structure. Fig. 3(b) matches our linearized analysis, with a quadratic log-prior density and coefficient design from Fig. 1. In several aspects of interior bone detail and narrow bone edge rendering this reconstruction has advantage over the previous. Finally, Figs. 3(c) and (d) result from applying the same coefficients to the q-GGMRF model. This result illustrates the greater tolerance to discontinuities of the q-GGMRF, while retaining the enhancement of the spatial frequency band as in the linear estimation case. The last image shows there little cost in reducing the size of the original spectral MRF design for reduced computation. In the optimization of these results, we monitored the second derivatives for the condition of (8), and found they remained positive throughout, despite the negative coefficients. Thus the non-convexity issue may be minor in practice.

## V. Conclusion

The MRF discussed has not been particularly carefully designed in order, or in frequency characteristic. Surely better results and/or lower order MRFs with similar results will be possible with further experimentation and analysis of bounds for convexity of the log *a posteriori* density. However, we have shown that some degree of useful manipulation of the spatial frequency response of Gaussian MRF-based Bayesian estimators is possible even with relatively simple design.

This result comes, of course, at the expense of added computation due to the larger neighborhood involved in each pixel's update. Reconstructions with the $11 \times 11$ neighborhood spectral design consumed approximately double the

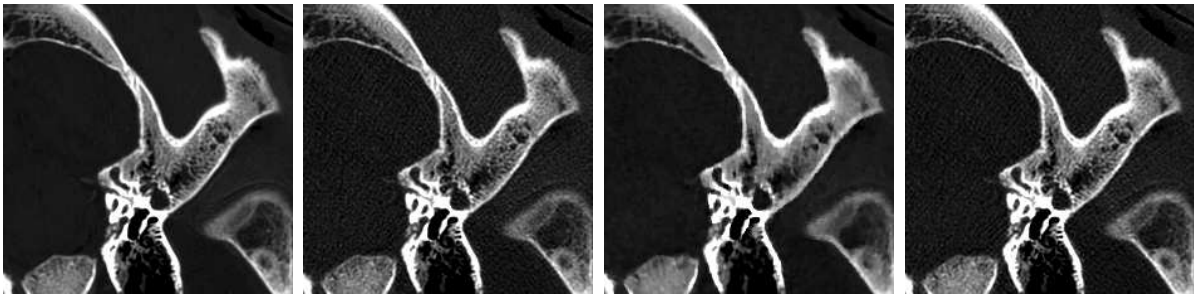

(a) (b) (c) (d)

Fig. 2. (a) "Ground truth" image, taken from high-dose scan of a pig cadaver's head; (b) filtered backprojection reconstruction using bone-enhancing filter; (c) MAP reconstruction with conventional image model and parameters adjusted for soft tissue rendering; (d) MAP reconstruction with spectral design of $11 \times 11$ MRF coefficients and Gaussian MRF model. Optimization was achieved with iterative coordinate descent.

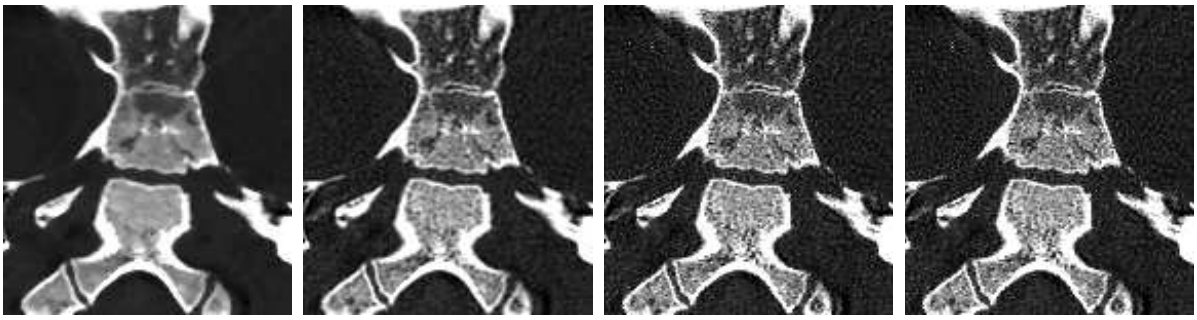

(a) (b) (c) (d)

Fig. 3. (a) MBIR reconstruction of clinical axial head reconstruction with conventional q-GGMRF; (b) MBIR with quadratic penalty, $11 \times 11$ spectrally designed MRF; (c) MBIR with q-GGMRF, $11 \times 11$ spectrally designed coefficients. (d) same, with $7 \times 7$ neighborhood.

reconstruction time of the conventional MRF estimate in a straightforward serial implementation, although this could be efficiently optimized on modern hardware. An adaptive implementation, which could apply these more complicated priors parsimoniously, may also eliminate the majority of that cost. The degree to which the iterative forward and backward projection operations dominate computational cost will affect the relative computational penalty such modeling enhancements incur.

## ACKNOWLEDGMENT

This research was supported by GE Healthcare.

## REFERENCES

[1] D. Politte, S. Yan, J. O'Sullivan, D. Snyder, and B. Whiting, "Implementation of alternating minimization algorithms for fully 3D CT imaging," in *Proc. of SPIE/IS&T Symp. Computat. Imag. II*, San Jose, CA, Jan. 17-18 2005, pp. 362–373.

[2] M. Knaup, W. Kalendar, and M. Kachelriess, "Statistical cone-beam CT image reconstruction using the cell broadband engine," in *Proc. of IEEE Medical Imaging Conference*, San Diego, CA, October 29 - November 5 2006.

[3] A. Ziegler, T. Köhler, and R. Proksa, "Noise and resolution in images reconstructed with FBP and OSC algorithms for CT," *MP*, vol. 34, no. 2, pp. 585–598, 2007.

[4] G. Wang, Y. Yu, and B. DeMan, "An outlook on X-ray CT research and development," *Medical Physics*, vol. 35, no. 3, pp. 1051–1064, 2008.

[5] S. Do, M. Kalra, Z. Liang, W. Karl, T. Brady, and H. Pien, "Noise properties of iterative reconstruction techniques in low-dose CT scans," in *Proc. SPIE Phys. Med. Imag.*, vol. 7258, no. 1, June 2009, pp. 808–814.

[6] Z. Yu, J.-B. Thibault, C. Bouman, K. Sauer, and J. Hsieh, "Fast model-based X-ray CT reconstruction using spatially nonhomogeneous icd optimization," *IEEE Trans. on Image Processing*, vol. vol. 20, no. 1, pp. 161–175, January 2011.

[7] J. Besag, "Spatial interaction and the statistical analysis of lattice systems," *Journal of the Royal Statistical Society B*, vol. 36, no. 2, pp. 192–236, 1974.

[8] S. Lakshmanan and H. Derin, "Valid parameter space for 2-D Gaussian Markov random fields," *IEEE Trans. on Information Theory*, vol. 39, no. 2, pp. 703–709, March 1993.

[9] S. Silvey, *Statistical Inference*. London: Chapman and Hall, 1975.

[10] D. Geman and G. Reynolds, "Constrained restoration and the recovery of discontinuities," *IEEE Trans. on Pattern Analysis and Machine Intelligence*, vol. 14, no. 3, pp. 367–383, 1992.

[11] M. Nikolova, J. Idier, and A. Mohammad-Djafari, "Inversion of large-support ill-posed linear operators using a piecewise gaussian MRF," *IEEE Trans. on Image Processing*, vol. 7, no. 4, pp. 571–585, April 1998.

[12] J.-B. Thibault, K. Sauer, C. Bouman, and J. Hsieh, "A three-dimensional statistical approach to improve image quality for multi-slice helical CT," *Medical Physics*, vol. 34, no. 11, pp. 4526–4544, November 2007.